Mon. Not. R. astr. Soc. (1974) **166,** 585–616.

DYNAMICAL MODELS FOR THE FORMATION AND EVOLUTION OF SPHERICAL GALAXIES

Richard B. Larson

(Received 1973 September 21)

SUMMARY

Models for the collapse of spherical protogalaxies have been computed using a two-fluid hydrodynamical approach to treat both the gas and the stars. The effects of gaseous energy losses, star formation, stellar mass loss and heavy element (Z) production are included and are followed over the lifetime of the galaxy. With reasonable choices for the parameters, the models reproduce well the observed structure of NGC 3379 and other nearly spherical galaxies. The observed Z gradients in elliptical galaxies are qualitatively reproduced, and metal-poor stars are very rare in the inner regions of the models, as in the solar vicinity. Star formation continues for the longest time in the nucleus, owing to the continuing condensation of residual gas toward the centre, and in some circumstances the infall of the last remnants of the initial protocloud may continue to support significant star formation in a galaxy even after 10^{10} yr. Various characteristics of the models suggest that the quasar phenomenon may be identifiable with the formation of the nucleus of a giant elliptical galaxy.

1. INTRODUCTION

As our knowledge about galaxies has steadily increased, it has become more and more clear that many of the most basic properties of galaxies can only be explained through an understanding of how they were formed. For example, because of the very long relaxation times of galaxies, such basic structural properties as the degree of flattening and the degree of central concentration can hardly change significantly after a galaxy has formed, and must therefore be determined at the time of formation. Also, the basic properties of the stars in a galaxy, such as the stellar metal abundances and their variation with position in the galaxy, are largely determined at the time of formation of the system. It is therefore of considerable interest to try to construct theoretical models describing the formation and evolution of galaxies and capable of predicting in some detail the various properties of interest.

The most widely accepted point of view concerning the origin of galaxies is that they have formed through the collapse of ' protogalaxies ', or relatively dense regions in the early universe which were gravitationally bound and therefore stopped expanding and collapsed to form galaxies within 10^{10} yr after the initial big bang (Rees 1971; Field 1974). At present, the origin and the properties of the dense regions which eventually collapse to form galaxies are not well understood, so that in order to compute models for the formation and evolution of galaxies it is necessary to postulate somewhat arbitrarily the existence of protogalaxies with suitable properties. Recently some attention has been devoted to cosmologies in

which it is assumed that the Universe was initially quite chaotic and that the present galaxies and clusters of galaxies represent the surviving vestiges of the primordial chaos; possibly the further development of such theories will be able to account in a natural way for the basic properties of galaxies (Rees 1971). The possible role of primordial turbulence in the formation of galaxies has been investigated by Silk & Ames (1972) and Jones (1973), and these authors conclude that primordial turbulence may well be able to produce protogalaxies with the required properties, although a complete theory of protogalaxy formation based on primordial turbulence is not yet available.

In the present investigation we are mainly concerned with the processes occurring in a protogalaxy of typical galactic mass ($10^{11}\ M_\odot$) after it has stopped expanding and has begun to collapse to form a galaxy. Dynamical calculations similar to the present ones were previously carried out by Larson (1969, Paper I) and were shown to be able to provide a good qualitative representation of the observed structure of elliptical galaxies. Recent improvements in the quantity and quality of observational data on elliptical galaxies have made it desirable to calculate more detailed models capable of predicting not only the structure of a galaxy but also the metal abundance and photometric properties of the galaxy as a function of distance from the centre. In addition, various cosmological studies require a detailed knowledge of how the properties of a galaxy vary with time from the time of formation to the present. In order to be able to provide such predictions, the present model calculations are improved over those of Paper I by the inclusion of the effects of stellar evolution, stellar mass loss, and heavy element production throughout the lifetime of a galaxy, as described in Section 3. Also, since the dynamical assumptions of Paper I were somewhat arbitrary and difficult to justify physically, some different and possibly more realistic dynamical assumptions have been considered in the present models, as described in Section 2.

The basic question to which this investigation has been directed is whether collapse models of the present type, based on simple and plausible assumptions, can explain satisfactorily the principal observed properties of typical elliptical galaxies. Other questions of interest include the question of whether the effect of gas flows during the galaxy formation process can produce a metal abundance distribution like that observed in the solar neighbourhood, where metal poor stars are quite rare (Larson 1972b; Searle 1973). It is also of interest to consider the probable time (i.e. redshift) and observational consequences of the galaxy formation process, and in particular to consider whether the quasar phenomenon can be interpreted as a stage in the formation of a galaxy, as suggested by Field (1964). A related question is that of whether it is possible in some cases for the condensation of protogalactic matter into a galaxy to continue for an extended period of time and produce significant observable effects even after 10^{10} yr (Larson 1972a). Finally, there is the problem of explaining the apparent correlation between the mass and the metal abundance of elliptical galaxies (Sandage 1972; Faber 1973). It is not yet possible to give definitive answers to all of these questions, but in most cases the present model results are able to provide at least some partial or suggestive answers.

The present paper will be concerned mainly with the dynamical and chemical properties of the various models considered. The photometric properties of these models have been computed by B. M. Tinsley, and they will be described in detail and compared with the observations in a later paper.

2. DYNAMICAL ASSUMPTIONS

2.1 *General assumptions*

For computational reasons it is necessary to adopt a number of idealizing assumptions concerning the model protogalaxies to be studied. We shall consider only spherically symmetric, non-rotating models, and we assume that a protogalaxy can be treated as a discrete, isolated system with a boundary enclosing a fixed mass, most or all of which eventually collapses into a galaxy. Thus we neglect any interactions or mass exchange between a protogalaxy and its surroundings. We also neglect the possibility that a galaxy may form by the clustering or agglomeration of smaller objects (Saslaw 1972). At present we cannot argue that such processes are unimportant, but only that one must first solve the simpler problem of what would happen in their absence. The resulting models for the formation and evolution of isolated spherical galaxies will hopefully provide a reasonable representation not only for spherical galaxies but also for moderately flattened elliptical galaxies as well, since the basic properties of moderately flattened ellipticals do not appear to differ much from those of spherical galaxies. It may also be hoped that when the effects of finite angular momentum are taken into account, certain of the present results can be extended to the case of flattened rotating systems; this expectation is in fact borne out by some preliminary results for rotating models, to be published in a later paper.

2.2 *The two-fluid representation*

The dynamics of the gaseous and stellar components of a collapsing protogalaxy have been calculated in the same way as in Paper I; that is, the gaseous and stellar components have been treated as two independent fluids for which fluid-dynamical equations can be derived by taking moments of the Boltzmann equation. The resulting equations describe the variation of the fluid-dynamical variables, i.e. the local mean density, the mean velocity, and the velocity dispersion, for the gas and the stars as functions of time and radial coordinate r. The gas is assumed to be clumpy and turbulent, with large (supersonic) internal mass motions that provide the dominant contribution to the velocity dispersion. In Paper I it was rather arbitrarily assumed that the gas is concentrated into discrete spherical clouds with masses equal to the Jeans mass; the number of such clouds is then so large that the local average values of the gas density, mean velocity and velocity dispersion are reasonably well defined and can be used in a fluid-dynamical treatment. Unfortunately, it is difficult to justify the assumption that the inhomogeneities and internal motions in the gas are all of a scale much smaller than the galaxy, since the gas may in reality contain inhomogeneities and streaming motions on all scales up to that of the galaxy itself; if so, it would become difficult to define local mean values of the fluid variables, and a spherically symmetric fluid-dynamical description of the gas would be only a crude approximation to reality. Nevertheless, this approach should still yield results that are at least qualitatively valid, and it may in any case be all that is warranted by our still very sketchy understanding of most of the detailed physical processes involved in the formation and evolution of galaxies.

2.3 *The gaseous dissipation and star formation rates*

A model for the formation of a galaxy must incorporate some description of the two principal physical processes involved: (1) the dissipation of the internal

motions in the gas, a process which plays an important role in allowing the gas to condense, and (2) the continual transformation of gas into stars. Since our understanding of these processes is still inadequate to allow us to calculate their rates in any *a priori* way, it is necessary to make some plausible assumptions. In Paper I the gaseous dissipation rate was obtained from the discrete cloud model for the turbulent motions, and the star formation rate was assumed to depend on a power of the gas density. Since these assumptions are rather arbitrary and not justified by any strong physical arguments, we have in some of the present calculations adopted different assumptions which are simpler and perhaps more physical; these are described below.

Instead of assuming that all of the internal motion in the gas is in the form of small scale cloud motions, it may be more realistic to assume that the gas is in general characterized by streaming motions on all scales up to that of the galaxy itself; most of the kinetic energy of the gas may then be in motions whose scale is not much smaller than that of the galaxy. This possibility is suggested in part by the fact that most galaxies are observed to rotate, and some show more complicated internal motions; thus protogalaxies must have contained at least some large scale internal motions, and these may have been quite chaotic. If most of the gaseous dissipation occurs through collisions between large scale gas streams, the dissipation time will be comparable to the time scale for these streaming motions, which is approximately the dynamical or free fall time for the system. We have therefore assumed that the rate of dissipation of the kinetic energy of internal motions in the gas is related to the dynamical time scale by

$$\frac{1}{\alpha_g}\frac{d\alpha_g}{dt} = -C_D t_f^{-1}, \tag{1}$$

where α_g denotes, as in Paper I, the mean square internal velocity of the gas in one coordinate direction, C_D is a dimensionless constant of order unity, and t_f is a local free fall time defined by

$$t_f = \left(\frac{3\pi}{32\, G\bar{\rho}}\right)^{1/2} \tag{2}$$

where $\bar{\rho}$ is the mean density of matter inside the radius r at which t_f is evaluated. C_D has been treated as a free parameter in the calculations, but it is found that reasonable results are obtained with values of C_D nearly equal to unity, as expected.

It is possible that the star formation rate, like the gaseous dissipation rate, is also determined by the large scale dynamics of the gas in a galaxy or protogalaxy. Observationally, this is suggested by the fact that star formation in galaxies usually occurs in spiral arms which, whatever their origin, evidently reflect large scale patterns in the dynamics of the gas. Recent theories have proposed that star formation is triggered by the compression of interstellar gas in spiral shock fronts; if so, the star formation rate is then determined, at least in part, by the rate at which the gas is processed through such shock fronts, and this is in turn related to the dynamical time scale of the galaxy. If protogalaxies and young galaxies contain large scale gas motions or streams, as we have assumed, then the shock fronts produced when these gas streams collide should likewise lead to star formation, and the time scale for the star formation process will again be related to the dynamical time scale for the system. Accordingly we have assumed that the star

formation rate, like the gaseous dissipation rate, is given by a relation of the form

$$\frac{1}{\rho_g}\frac{d\rho_g}{dt} = -C_S t_f^{-1} \tag{3}$$

where ρ_g is the gas density, $-d\rho_g/dt$ is the star formation rate, and C_S is a dimensionless constant of order unity. Again it is found that reasonable results are obtained with values of C_S near unity. It is evident that C_S cannot differ drastically from unity if the present prescription is to produce acceptable models, since if $C_S \gg 1$ star formation proceeds so rapidly that the gas is all transformed into stars before any strong central condensation has developed, whereas if $C_S \ll 1$ the gas collapses to a much too condensed configuration before forming stars.

It is not unreasonable that the star formation rate should be proportional to the gaseous dissipation rate, as implied by equations (1) and (3), since both processes involve inelastic compression of the gas and loss of energy by radiation. Indeed, if shock fronts are involved, the same shock fronts may be responsible for both dissipation and star formation. Of course, the above assumptions cannot be justified as valid in any more than an order-of-magnitude sense, so one cannot expect the resulting models to be quantitatively accurate in all respects, and it is mainly the qualitative features of the results which can be considered as well established and significant.

2.4 *Initial and boundary conditions*

Since we have essentially no observational information concerning the early properties of collapsing protogalaxies, it is necessary to adopt some more or less arbitrary assumptions for the initial and boundary conditions. In the present calculations, as in Paper I, we have considered two types of boundary conditions: (1) a boundary of fixed radius R, as might be appropriate for a galaxy forming in a cluster with approximately constant dimensions, and (2) a boundary expanding with time according to $R = R_0 t^{2/3}$, as might be appropriate for a field galaxy forming in an expanding region. While neither of these boundary conditions can be justified as being necessarily very realistic, the two cases should at least illustrate the range of possibilities that might plausibly occur.

In the case of a fixed boundary, as adopted in most of the calculations, the boundary radius R can be imagined to correspond approximately to the maximum radius attained by a protogalaxy before it begins to collapse. Since many elliptical galaxies are observed to extend out to radii of at least 30 kpc, a lower limit to the boundary radius is then approximately 30 kpc. An upper limit to a plausible boundary radius is set by the requirement that the collapse must be completed at a sufficiently early cosmological time. For example, if we assume that elliptical galaxies are at least 80 per cent as old as the Universe (i.e. that they formed at redshifts of the order of 2 or more), the maximum radius which a protogalaxy of mass $10^{11} M_\odot$ can attain before beginning to collapse is about 100 kpc. Most of the present calculations have been made for boundary radii of 30 or 50 kpc.

In all cases the protogalaxy has been assumed to consist initially entirely of gas, and to start with a uniform average density and velocity dispersion. The initial mean velocity of the gas has been taken to be zero in the models with a fixed boundary, and a uniform expansion in the cases with an expanding boundary. In reality, it is possible that a substantial fraction of the mass may already have been converted into stars when the protogalaxy begins to collapse (Gott 1973); however,

it appears that the presence of metal abundance gradients and highly condensed nuclei in elliptical galaxies can only be accounted for it at least some of the star formation occurred during or after the initial collapse. At any rate, the present results show that the observed properties of elliptical galaxies are consistent with the assumption that protogalaxies are still entirely gaseous when they begin to collapse. Since we have little idea what to assume for the initial velocity dispersion in a protogalaxy, this has been treated as a free parameter which can be adjusted to give the best agreement with observations. In the present models, values for the initial velocity dispersion ranging from 6 to 55 km s^{-1} have been considered.

3. STELLAR EVOLUTION, MASS LOSS AND HEAVY ELEMENT PRODUCTION

3.1 *Effects of stellar evolution*

Stars with masses greater than about 1 $M_\odot$ are believed to lose part of their mass at the end of their lifetime, and this stellar mass loss must be included in a complete model for the formation and evolution of a galaxy. The amount of mass lost from stars of different masses has been calculated on the assumption, following Tinsley (1972a) and Talbot & Arnett (1973), that stars with masses in the range $0{\cdot}7 < m < 5$ (solar units) leave a white dwarf remnant of mass 0·7, while stars of mass $m > 5$ leave a neutron star remnant of mass 1·4. The stellar lifetimes used in these calculations have been taken from Tinsley's (1972a) compilation of evolutionary lifetimes of stars of different masses. For computational convenience these tabulated lifetimes have been represented by the following simple analytic formula giving the stellar lifetime τ_m as a function of mass m:

$$\log \tau_m = 10{\cdot}02 - 3{\cdot}57 \log m + 0{\cdot}90 (\log m)^2 \qquad (4)$$

where τ_m is in years and m is in solar masses. This formula represents the tabulated lifetimes with a typical accuracy of about 5 per cent and a maximum error of about 15 per cent, which is probably consistent with the accuracy of the data.

Since the observable photomteric properties of a galaxy depend on the metal abundances of its stars, it is important to follow the production of heavy elements by massive stars during the evolution of the system. To calculate the amount of heavy elements ejected from stars of various masses we have used simple formulas supplied by B. M. Tinsley (private communication) and based on the assumptions of Talbot & Arnett (1973, Version I). The fraction of the total mass of a star of mass m which is ejected as heavy elements at the end of its lifetime is assumed to be given by

$$R_z = q_c + (1 - q_c) Z_f - 1{\cdot}4/m \qquad (5)$$

where Z_f is the metal abundance of the gas from which the star was formed and

$$q_c = 0{\cdot}156 + 0{\cdot}537 \log (m/9) \qquad (6)$$

is the fraction of the star's mass which is processed into a core of heavy elements during its lifetime. According to equation (6) the core mass $q_c m$ exceeds the assumed remnant mass of 1·4 only for stars of mass $m > 9$, so that only these stars actually release heavy elements to the surroundings when they die. Since stars of mass $m > 9$ have lifetimes $\lesssim 3 \times 10^7$ yr which are much shorter than the formation time of a galaxy ($\approx 10^9$ yr), the ejection of heavy elements can be considered as

taking place almost instantaneously after the formation of massive stars, so that the metal production rate is very nearly proportional to the star formation rate.

3.2 *The initial stellar mass spectrum*

Before any models can be calculated it is necessary to specify the mass spectrum with which stars are formed. In the absence of any direct knowledge of the stellar mass spectrum in external galaxies, a common practice has been to assume a simple parametric form for the mass spectrum, such as the power law adopted by Tinsley (1972a, b) for the number of stars formed per unit mass interval:

$$dN/dm \propto m^{-(1+x)} \tag{7}$$

where x is a free parameter, as are the upper and lower mass limits for the power law. The (non-dynamical) galaxy evolution models of Tinsley (1972a, b) show that the best agreement between the predicted and observed colours of elliptical galaxies is obtained with values of x between about 1·0 and 1·5; in particular, the well-known Salpeter law with $x = 1{\cdot}35$ gives results which agree well with the observations. Therefore we have adopted a Salpeter mass spectrum in most of the present models. The upper mass limit m_U has been taken to be 50 $M_\odot$, in approximate agreement with both the observed upper mass limit in the solar vicinity and the theoretical upper limit found by Larson & Starrfield (1971). While it is possible that some of the very first stars to form in a galaxy may have been much more massive than this limit because of the absence of heavy elements to cool the gas (Larson & Starrfield 1971), this would probably involve only a small fraction of the galaxy's mass, since as soon as even a small amount of heavy elements has been produced the gas temperature and the maximum stellar mass would be reduced to more ' normal ' values.

The choice of the lower mass limit m_L is more critical, since most of the galactic mass is in low mass stars; the choice of m_L thus determines both the mass-to-light ratio of the system and the fraction of the mass which goes into massive stars and is processed into heavy elements. In the present calculations values for m_L of 0·02 and 0·04 have been considered; values in this range appear to yield mass-to-light ratios and metal abundances which are approximately consistent with observations. It should be noted that m_L is not necessarily to be interpreted as an actual lower limit of stellar masses, since there is no reason to believe that the Salpeter law holds at such small masses; in effect, m_L is simply a parameter describing the fraction of the total mass which goes into very faint stars.

It would evidently be desirable to have a physical theory to predict the initial stellar mass spectrum, instead of having to rely on rather arbitrary formulas with several free parameters. An attempt in this direction has been made by Larson (1973) on the basis of a simple stochastic model of the fragmentation process. The resulting predicted mass spectrum, expressed as the fractional mass per unit logarithmic mass interval, is given by a gaussian function:

$$f(\log m) = \frac{1}{(2\pi)^{1/2}\, b} \exp\left[-\frac{(\log m - a)^2}{2b^2}\right] \tag{8}$$

where $f(\log m)$ is the fraction of the total mass per unit interval of $\log m$ and a and b are the mean and standard deviation of $\log m$. As an example, we have considered a gaussian mass spectrum with $a = 0$ and $b = 0{\cdot}75$; this is similar to the one which

was found by Larson (1973) to approximate the available data for the initial mass spectrum in the solar vicinity. Since this choice of initial mass spectrum yields a mass-to-light ratio which seems somewhat too low for an elliptical galaxy and since recent data (e.g. Weistrop 1972) suggest the presence of more low mass stars in the solar vicinity than were previously known to exist, we have somewhat arbitrarily modified the gaussian mass spectrum by assigning only half of the total mass to the gaussian spectrum and the other half to unspecified 'invisible objects' of very low mass.

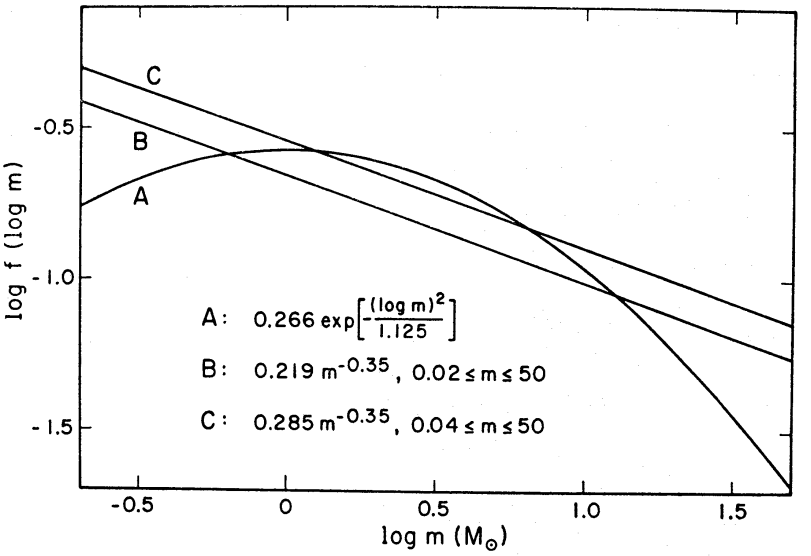

FIG. 1. *The three initial stellar mass spectra considered in the present models; $f(\log m)$ denotes the fraction of the total mass per unit interval of log m. A is a gaussian mass spectrum with mean 0 and standard deviation 0·75 in log m, multiplied by ½; B is a Salpeter mass spectrum with mass limits 0·02 and 50 $M_\odot$; and C is a Salpeter spectrum with mass limits 0·04 and 50 $M_\odot$.*

The three initial mass spectra considered in the present models are illustrated in Fig. 1, which shows $\log f(\log m)$ plotted *vs.* $\log m$. Curve A is the modified gaussian mass spectrum described above, curve B is a Salpeter mass spectrum with lower mass limit $m_L = 0{\cdot}02$, and curve C is a Salpeter spectrum with $m_L = 0{\cdot}04$. In all cases the initial mass spectrum has been assumed to remain the same at all places and times throughout the evolution of a galaxy. This assumption has been adopted mainly for simplicity and cannot be given any strong justification, but as will be seen, the results obtained with this assumption are consistent with the available observational data pertaining to galactic evolution.

4. CALCULATIONS

4.1 *Dynamical calculations*

In the present models, the gaseous component of a protogalaxy is characterized by a local mean density ρ_g, a mean velocity u_g, and a mean square internal velocity α_g, all of which are functions of r and t. The time variation of these quantities is governed by equations (I.12)–(I.14) of Paper I, here modified to include the effects of mass loss from evolving stars. The rate of mass ejection from stars per unit volume, $d\rho_e/dt$, is calculated as described below in Section 4.3, and this quantity

is added to the right-hand side of the continuity equation (I.12) to represent an input of gas. If u_e denotes the mean velocity of the ejected gas, conservation of momentum requires that the term $(u_e-u_g)(d\rho_e/dt)/\rho_g$ be added to the right-hand side of the momentum equation (I.13); likewise, if α_e is the mean square velocity of the ejected gas, conservation of energy requires the term $(\alpha_e-\alpha_g)(d\rho_e/dt)/\rho_g$ to be added to the right-hand side of the energy equation (I.14).

The choice of values for u_e and α_e is not entirely trivial and requires some discussion. Since much of the ejected gas comes from short-lived massive stars which have mean velocities closer to the gas velocity u_g than to the average stellar velocity u_s, u_e will not be equal to u_s but will be intermediate between u_s and u_g. Since the exact choice of u_e does not appear to be of critical importance for the dynamics, we have simply set u_e equal to $\frac{1}{2}(u_s+u_g)$. It is more difficult to estimate α_e, since this quantity represents the contribution of stellar mass ejection to the kinetic energy of large scale gas motions which are mostly of a much larger scale than the gas shells ejected from individual stars. It is possible that the kinetic energy of the ejected shells is completely dissipated on small scales and makes no contribution to the large scale motions of the gas, in which case $\alpha_e \approx 0$. On the other hand, if the young stars responsible for most of the mass ejection retain some of the streaming motions of the gas from which they formed, the ejected material will likewise possess some large scale motions whose velocity dispersion may be comparable with that of the gas or the stars, in which case we might have $\alpha_e \approx \alpha_s$. It is even possible that very energetic ejection processes could make α_e much larger than α_s. In the present models we have not attempted to include such effects, but have simply assumed $\alpha_e = \alpha_s$. In practice, the effect of varying the assumed value of α_e is found to be similar to the effect of varying C_D in equation (1), so the uncertainty in α_e can be regarded as being partially absorbed into the free parameter C_D.

The stellar component of a protogalaxy is characterized by four variables: a mean density ρ_s, a mean velocity u_s, and the mean square random velocities α_s and β_s in the radial and transverse directions. The evolution of these quantities is governed by equations (I.15)–(I.18) of Paper I, with the single modification that here the stellar mass loss rate, $-d\rho_e/dt$, is added to the right-hand side of the continuity equation (I.15). The complete set of modified dynamical equations for the gas and the stars can then be solved in exactly the same way as in Paper I.

4.2 *The star formation history*

In order to calculate the stellar mass loss and metal production rates and the photometric properties of a galaxy at any time in its evolution, it is necessary to keep track of the distribution of stellar ages and initial metal abundances as functions of position and time throughout the evolution of the system. If the mean motion of the stars could be neglected, i.e. with $u_s = 0$, this could be accomplished by simply storing the star formation rates (or density increments) and the initial stellar metal abundances calculated for each zone during each time step. In general, however, it is necessary to take into account the fact that the stars do not remain in the same zones in which they were formed but move radially with average velocity u_s. It is also desirable to allow for the fact that the youngest stars, which account for most of the mass ejection, have mean velocities closer to the gas velocity u_g than to the average stellar velocity u_s. We have crudely allowed for this by assigning a different mean velocity u to the stars in each age group, varying continuously from

$u = u_g$ for newly formed stars to $u = u_s$ for old stars. In particular, we have assumed that u varies linearly with stellar age τ for $0 < \tau < t_f$ and that $u = u_s$ for $\tau > t_f$, where t_f is the free fall time defined by equation (2) and is taken to be the effective mixing time for stellar velocities. Using the mean velocities estimated in this way for stars in each age group, the flux of stars in each group across the zone boundaries has been calculated using equation (I.22) of Paper I at each time step.

After the above procedure has been carried out, the star formation rates (or density increments) stored for each previous time step give the complete past history of star formation for those stars currently located in each zone; this is clearly the information required to calculate the mass ejection rate and photometric properties for each zone. In practice, the time steps originally used in the dynamical calculations have been merged into a smaller number of time intervals for which averaged star formation data have been kept stored; this has been done in order to economize on the computing and storage demands. Merged time intervals not less than about one-tenth of the initial free fall time were found to provide coarse but adequate time resolution for the history of star formation throughout the evolution of the system.

It should be noted that only the mean motions of the stars have been taken into account in these models; the effects of the random orbital motions of individual stars, which would result in some spatial diffusion or mixing of stellar characteristics, are not taken into account in the present models.

4.3 *The stellar mass loss and metal production rates*

In calculating the stellar mass loss and heavy element production rates, the stars have been divided into a large number of mass intervals (typically about 60), chosen to be much smaller near 1 $M_\odot$ than at larger masses so as to keep the difference in stellar lifetimes between neighbouring mass groups less than 10^9 yr; this is necessary to ensure adequate time resolution in calculating the required time integrals. For each mass interval, equation (4) gives the corresponding interval of lifetimes τ_m and hence the interval of formation times $t - \tau_m$ for those stars which at time t are just ending their lifetimes and ejecting mass. For each stellar mass the fractional mass which is lost at the end of a star's lifetime is known, given the assumed remnant mass (Section 3.1). Multiplying the fractional mass loss by the rate at which stars of each mass die, which is the same as the rate at which they were formed at a time τ_m earlier, it is straightforward to calculate the total mass loss rate $d\rho_e/dt$ by integrating the star formation rate over the time interval of formation for each mass group and then adding the contributions of all mass groups. This calculation makes use of the star formation rates stored for the previous time intervals of the evolution, and in evaluating the time integrals the star formation rate is assumed to be constant during each time interval and the distribution of stellar lifetimes is taken to be uniform within each mass interval. The rate of production of heavy elements $d\rho_z/dt$ is calculated in the same way as the mass loss rate $d\rho_e/dt$, using equations (5) and (6) to calculate for each stellar mass the fractional mass which is ejected as heavy elements, and using stored data for the initial stellar metal abundances Z_f in each zone.

4.4 *Metal abundances of the gas and stars*

The metal abundance Z_g of the gas is by definition equal to ρ_z/ρ_g where ρ_z is the density of heavy elements in the gas. Differentiating with respect to time, we

obtain the following expression for the Lagrangian rate of change of Z_g due to metal production at the rate $d\rho_z/dt$ and mass loss at the rate $d\rho_e/dt$:

$$\frac{dZ_g}{dt} = \frac{1}{\rho_g}\left(\frac{d\rho_z}{dt} - Z_g\frac{d\rho_e}{dt}\right). \tag{10}$$

The corresponding Eulerian equation used to calculate the time variation of Z_g is

$$\frac{\partial Z_g}{\partial t} + u_g\frac{\partial Z_g}{\partial r} = \frac{1}{\rho_g}\left(\frac{d\rho_z}{dt} - Z_g\frac{d\rho_e}{dt}\right). \tag{11}$$

Equation (11) has been replaced by an implicit difference approximation of the same form as those used in the dynamical calculations, as described in Paper I. In calculating the change in Z_g during each time step the quantities $d\rho_z/dt$ and $d\rho_e/dt$ have been calculated as described in Section 4.3 at the beginning of the time step, and they have been assumed to remain constant during the time step. Since the dynamical equations are independent of Z_g, the dynamical variables can be advanced first and the new values of u_g and ρ_g thus obtained can be used in equation (11). All of the quantities in equation (11) are then known except for Z_g, and new values for Z_g can be calculated by solving the resulting simple set of linear equations.

The average stellar metal abundance Z_s is calculated from an equation similar to (11), except for the source term on the right-hand side which in this case gives the rate of change of Z_s due to star formation at the rate $d\rho_s/dt$ from gas with metal abundance Z_g:

$$\frac{\partial Z_s}{\partial t} + u_s\frac{\partial Z_s}{\partial r} = \frac{(Z_g - Z_s)}{\rho_s}\frac{d\rho_s}{dt}. \tag{12}$$

Once Z_g has been calculated, all of the quantities in equation (12) are known except for Z_s, and the difference approximation to equation (12) can be solved for new values of Z_s in the same way as the equation for Z_g. In this case a consistency check on the accuracy of the calculations can be performed by comparing the value of Z_s calculated from equation (12) with that calculated from the stored data for the star formation rates and initial stellar metal abundances in each zone. The two values for Z_s are generally found to agree to an accuracy of about 10–20 per cent, although in a few exceptional situations discrepancies of up to 50 per cent may occur. In view of the various uncertainties affecting both the theory and the observations relating to metal abundances in galaxies, this appears to be an acceptable level of numerical accuracy for the present purposes.

5. RESULTS AND COMPARISON WITH OBSERVATIONS

5.1 *Structure of the resulting galaxy*

We consider first the results obtained for models constructed with the simplest possible assumptions, i.e. models for which the boundary radius R is fixed and the gaseous dissipation and star formation rates are given by equations (1)–(3). Apart from scale factors for the mass and radius, there are then three principal parameters which determine the dynamical properties of the models: the constants C_D and C_S in equations (1) and (3), and the ratio of the initial velocity dispersion to the velocity dispersion given by the virial theorem. The choice of initial stellar mass spectrum also influences the dynamics through its effect on the stellar mass loss

rate, but for the cases considered here this is not an important source of variability between the models, and it has in any case been largely compensated by small adjustments to the constant C_S specifying the star formation rate.

Since the constants C_D and C_S and the initial velocity dispersion cannot be predicted quantitatively, these quantities have been treated as free parameters to be varied until the best match between the model predictions and the observed properties of elliptical galaxies is found. The most extensively observed property of elliptical galaxies is the surface brightness distribution $I(r)$; for a constant mass-to-light ratio, this is proportional to the projected surface density $\sigma(r)$, a quantity which can be directly calculated from the stellar density distribution $\rho_S(r)$ of any model. The only elliptical galaxy for which extensive photoelectric surface brightness measurements have been published appears to be the E1 galaxy NGC 3379 studied by Miller & Prendergast (1962). Recent unpublished observations by I. R. King (private communication) of 15 elliptical galaxies show that most of these galaxies have luminosity profiles quite similar to that found by Miller & Prendergast (1962) for NGC 3379; we have therefore adopted NGC 3379 as a standard with which to compare the model predictions.

A series of three models designated Models A, B and C have first been calculated with the initial stellar mass spectra A, B and C of Section 3.2 and Fig. 1 in order to find out how the results depend on the initial mass spectrum. These models all have an assumed boundary radius of 30 kpc, which is probably a lower limit for the maximum radius attained by a typical protogalaxy. Since the three models are found to be dynamically almost identical, and since Model B seems to give the best fit to the observed photometric properties of NGC 3379, we describe first the results for Model B which has a Salpeter mass spectrum with lower mass limit $0{\cdot}02\ M_\odot$. For this model, it is found that good agreement between predicted and observed projected density distributions is obtained with values of C_D and C_S near unity, i.e. $C_D = 0{\cdot}85$ and $C_S = 0{\cdot}90$, and with an initial velocity dispersion of 12 km s^{-1}.

The density distributions for the stars and gas in Model B after an assumed galactic lifetime of 12×10^9 yr are illustrated in Fig. 2. The predicted stellar density distribution is approximately of the form $\rho \propto r^{-2{\cdot}65}$ for radii between about 300 pc and 20 kpc, a range which includes the bulk of the galaxy's mass. The density does not reach a flat maximum at the centre as in the models of Paper I but increases steadily to the smallest radius used in the calculations (about 0·1 pc), approximately as $r^{-0{\cdot}75}$. This steady increase in density at small radii is not necessarily realistic, since the model assumptions are probably not valid on such small scales; nevertheless, it is worth noting that the small dense core predicted by this model resembles the dense cores actually observed in M31 and M32. For example, M32 has a small core with a radius of ~ 8 pc and a mass of $\sim 10^7\ M_\odot$ (Walker 1962); for comparison, Model B has a mass of about $4 \times 10^6\ M_\odot$ in a region of the same size.

The projected stellar density distribution of Model B is illustrated in Fig. 3, where it is compared with the surface brightness measurements of NGC 3379 by Miller & Prendergast (1962), reduced in the same way as by King (1966). The theoretical curve has been positioned to give the best fit to the observations, but the horizontal placement of the curve is close to that appropriate for a distance to NGC 3379 of 14·6 Mpc, as would be implied by the measured redshift of 730 km s^{-1} with a Hubble constant of 50 km s^{-1} Mpc^{-1}. The fit is seen to be rather good, demonstrating that simple collapse models with apparently reasonable choices of

parameters are able to reproduce in some detail the observed radial structure of typical elliptical galaxies like NGC 3379. As would be expected, the space density distribution $\rho \propto r^{-2.65}$ projects into a surface density distribution which is approximately $\sigma \propto r^{-1.65}$ over much of the galaxy. The predicted increase in $\sigma(r)$ at small radii is possibly in conflict with the observations which suggest a flat central maximum, but the observations are limited to a resolution not much better than 100 pc (1·4″) and therefore cannot rule out the presence of a small sharp core at the centre of NGC 3379.

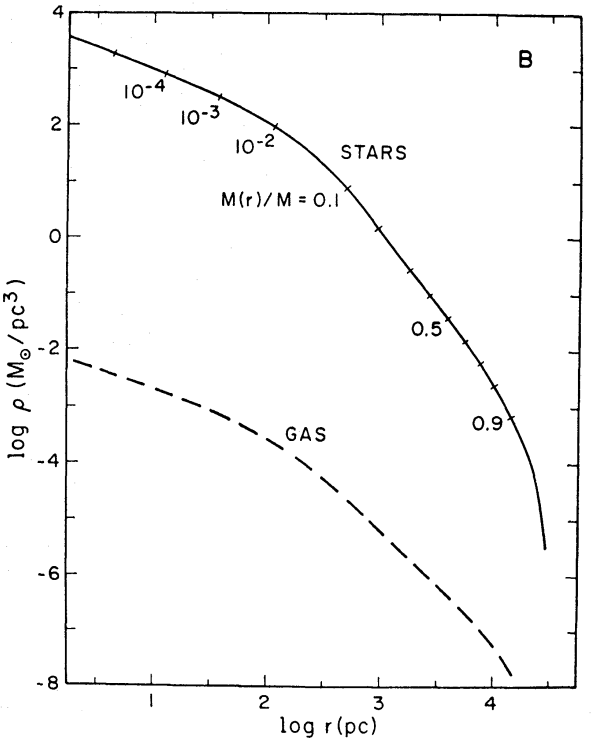

FIG. 2. *The density distributions of the stars and gas in Model B at* $t = 12 \times 10^9$ *yr. The radii enclosing various fractions of the total mass are marked along the solid curve. The total mass is* $10^{11}\ M_\odot$, *of which* $1{\cdot}4 \times 10^6\ M_\odot$ *is still in gaseous form.*

Both the model and the observations show a possibly significant slight change in slope near $r \sim 1{\cdot}5$ kpc. In the model this represents a dividing point between two dynamically distinct regions which may be referred to as the ' halo ' and the ' nucleus '. The ' halo ' part of the galaxy consists mostly of stars formed during the initial free fall stage of the collapse, which thus have radially elongated orbits with a ratio of radial to transverse velocity dispersions of about 3 at $r = 10^4$ pc. The ' nucleus ', on the other hand, consists mostly of stars formed after the velocity dispersion of the gas has built up sufficiently to slow or halt the initial free fall collapse near the centre, so that the stars in this region are formed in a near equilibrium configuration and have a nearly isotropic velocity distribution.

In order to determine the importance of the assumed boundary radius R, we have computed Model D with the same initial mass spectrum as Model B but with a boundary radius of 50 kpc which may be more realistic than the 30 kpc assumed for Models A–C. The other parameters for Model D are $C_D = 0{\cdot}75$, $C_S = 0{\cdot}80$, and an initial velocity dispersion of 5·7 km s^{-1}. The results for Model D

are in most respects quite similar to those for Model B, except that the collapse time scale is increased by a factor of 2·2; thus the initial free fall time is increased from $2{\cdot}7 \times 10^8$ yr to $5{\cdot}9 \times 10^8$ yr. The projected density distribution of Model D, illustrated in Fig. 8, is quite similar to that of Model B except that it falls off less rapidly at radii larger than about 6 kpc, where it does not fit the observations of NGC 3379 quite as well as does Model B. However, it is worth noting here that NGC 3379

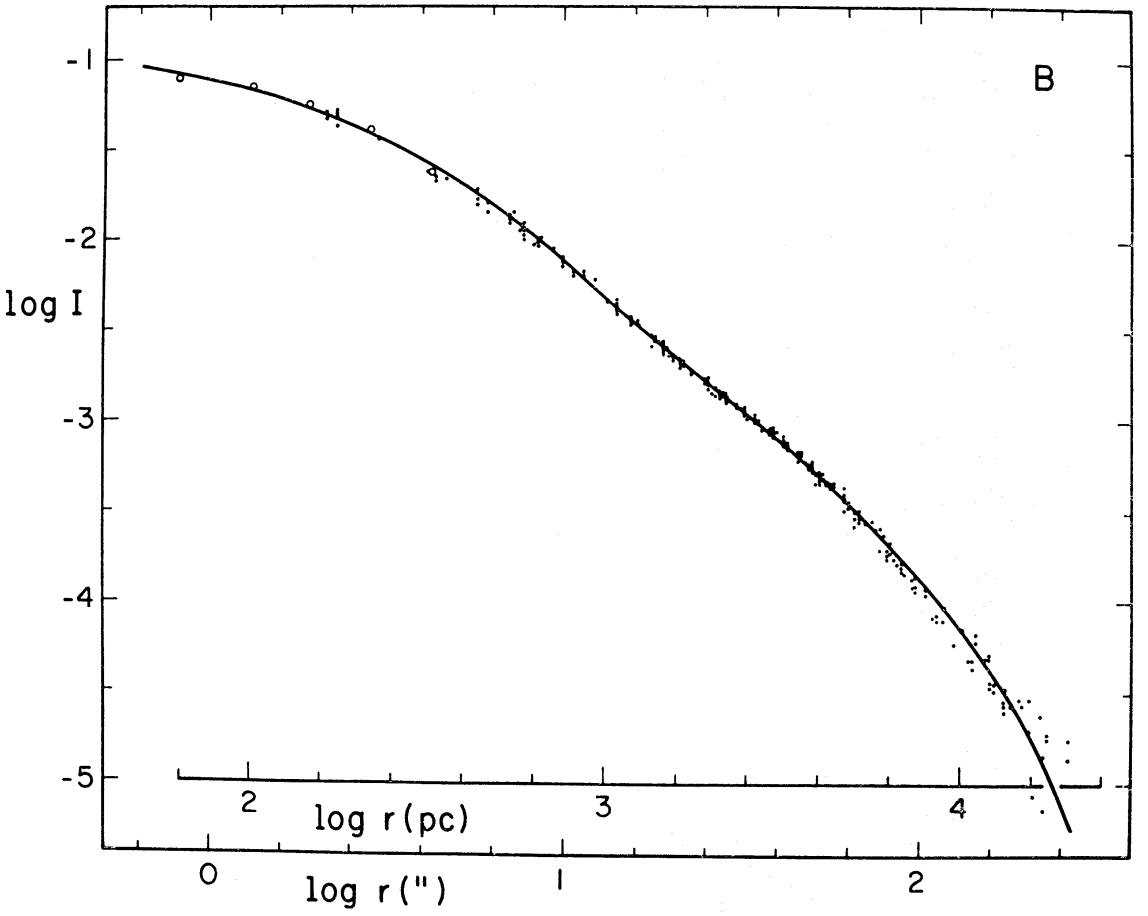

FIG. 3. *The projected density distribution of Model B (solid curve) compared with the V-magnitude surface brightness measurements of NGC 3379 by Miller & Prendergast (1962). Here I denotes the ratio of the number of galaxy counts per square arcsecond aperture to the number of reference star counts, and the slight ellipticity of the image has been corrected for in the same way as by King (1966). The dots are direct measurements and the open circles are deduced from measurements made with different apertures centred at the centre of the galaxy. The curve has been shifted to give the best fit to the observations; the horizontal placement corresponds to a distance of 15·8 Mpc, and the vertical placement corresponds to* $\sigma(r) = 7{\cdot}2 \times 10^5\, I(r)\, M_\odot\, pc^{-2}$.

has a close companion galaxy, NGC 3384, which probably influences its outer structure; other more isolated elliptical galaxies have luminosity profiles which on the average fall off slightly less rapidly than NGC 3379 at large radii (King, private communication), and in some cases they extend out to radii of the order of 50 kpc or more. The mean profile of 14 elliptical galaxies as determined by King is, in fact, matched better by Model D than by Model B at large radii.

The projected stellar velocity dispersion in Model D, which is nearly identical to that in Models A–C, is shown as a function of projected radius in Fig. 10. The

velocity dispersion predicted for the nuclear region is in good agreement with the observed nuclear velocity dispersion of 187 km s^{-1} in NGC 3379 (Burbidge, Burbidge & Fish 1961), confirming that the mass of NGC 3379 is indeed about $10^{11}\,M_{\odot}$, as assumed.

The residual gas content of Models A–D after 12×10^{9} yr is of the order of $2\times10^{6}\,M_{\odot}$, most of which is in the outer regions of the galaxy and at extremely low densities; under these conditions it appears that this amount of gas would be unobservable, in agreement with the absence of any observable gas content in most elliptical galaxies.

5.2 *Metal abundances and photometric properties*

To obtain a quantity that can be compared with observations of metal abundances in elliptical galaxies, we have calculated a ' projected metal abundance Z_p by averaging the stellar metal abundance Z_s along each line of sight through each model. Fig. 4 shows the resulting Z_p distributions for Models A–C at an assumed galactic age of 12×10^{9} yr. The three curves have the same shape and differ only by scale factors depending on the initial stellar mass spectrum; as is evident from Fig. 1, Models A, B and C have increasing proportions of massive stars in the initial mass spectrum, and therefore they show increasing final metal abundances. The + symbols plotted in Fig. 4 represent crudely calibrated metal abundance measurements for the nuclear region of NGC 3379, derived from the CN band observations of Spinrad *et al.* (1972); the plotted points have been derived from Table 2 of Spinrad *et al.* (1972) by assuming rather arbitrarily that a ' super metal rich ' star has $Z = 0{\cdot}06$ and a ' normal ' star has $Z = 0{\cdot}015$.

The most striking feature of Fig. 4 is that both the models and the observations show a steep radial gradient in metal abundance in the nuclear region ($r \lesssim 2$ kpc). The reason for the abundance gradient in the models is readily understood in terms of the dynamics of formation of the nuclear region. The stars in this region

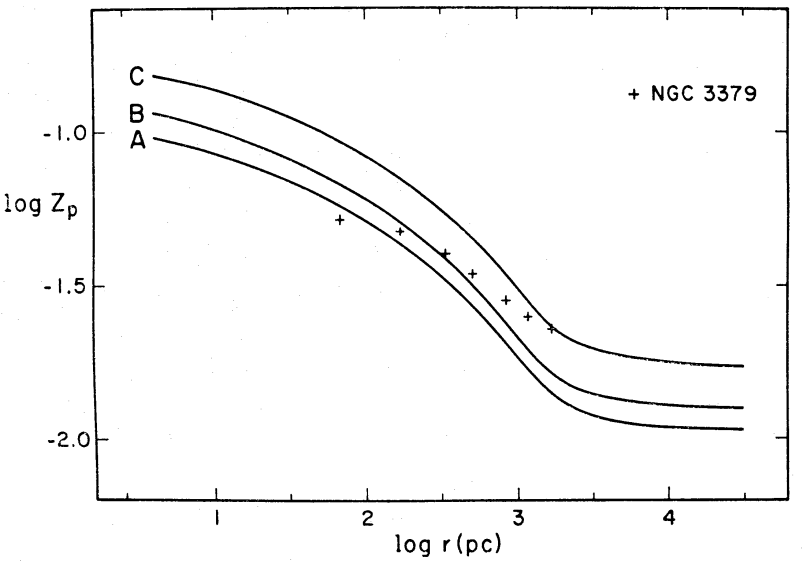

FIG. 4. *The stellar metal abundance averaged along lines of sight through Models A, B and C and plotted* vs. *projected distance from the centre. The + symbols are derived from observations of NGC 3379 by Spinrad et al.* (1972, *Table 2*) *by assuming that a ' super metal rich ' star has* $Z = 0{\cdot}06$ *and a ' normal ' star has* $Z = 0{\cdot}015$.

are formed with a velocity dispersion which is nearly large enough to balance gravity, and therefore they experience little net inward motion after they are formed. In contrast, the gas continues to dissipate its kinetic energy and condense centrally through the stellar background. The heavy elements ejected by evolving stars are therefore carried inward by the inflowing gas, and the gas becomes more and more enriched in heavy elements as it flows toward the centre. Thus an abundance gradient is established in the gas, and this is reflected in the compositions of the stars which form from this gas.

The existence of metal abundance gradients and 'super metal rich' stars in the nuclei of many bright elliptical galaxies is now well established through the work of McClure (1969), Spinrad *et al.* (1971, 1972), and others. The fact that the present models predict such abundance gradients in a natural way adds further support to the general picture of galaxy formation represented by these models. Quantitatively, however, it is not yet possible to make accurate comparisons between predicted and observed metal abundances, since no accurate calibration of the observed photometric indices in terms of Z is yet available. Thus the apparent discrepancy in slope between the theoretical curves and the observations in Fig. 4 may not be significant. On the theoretical side, it should be noted that the models neglect the effects of stellar orbital motions which would tend to smear out the predicted abundance gradient and bring it closer to the 'observed' one.

In the 'halos' of Models A–D ($r \gtrsim 2$ kpc) the abundance gradient almost vanishes and the average stellar metal abundance becomes almost independent of r. This is because the halo stars are formed mostly during the initial free fall phase of the collapse when the gas and stars are falling inward together at nearly the same velocity; at this stage there is as yet little separation between gas and stars, and therefore little relative concentration of heavy elements toward the centre. At present there exist no measurements of CN bands or other metallicity indices at distances greater than about 2 kpc from the centres of elliptical galaxies, and therefore it is not known whether the metal abundances in galactic halos are really independent of r, as predicted for Models A–D. However, Miller & Prendergast (1962) found that the B–V colour of NGC 3379 is reddest at the centre and becomes bluer with increasing radius out to about $r \sim 2$ kpc, beyond which point B–V becomes constant within the accuracy of measurement. If the colour variation is due to a variation in metal abundance, as seems most likely, then the absence of a colour gradient at $r \gtrsim 2$ kpc suggests that the metal abundance is indeed constant in this region of NGC 3379, as predicted for Models A–D.

From Fig. 4 it appears that Model B or perhaps something intermediate between B and C may provide the best match to the 'observed' metal abundance of NGC 3379, although this comparison is rather uncertain. A further important check or constraint on the models is provided by the photometric properties of the models, which have been computed by B. M. Tinsley and will be described in detail in a later paper. These calculations show, for example, that Models B and C both have B–V colours of about 0·97 in the 'halo' region, in excellent agreement with the observed B–V of 0·96 for the halo of NGC 3379 (Miller & Prendergast 1962). Model A, with B–$V \simeq 0{\cdot}94$, is slightly but probably not significantly bluer, so that all three models predict colours which are in satisfactory agreement with the observations. The mass-to-light ratio M/L_B has also been calculated and is about 20 for Model A, 24 for Model B and 17 for Model C; within the considerable uncertainty, all of these values are consistent with the observed mass-to-

light ratios for elliptical galaxies, which are believed to be typically of the order of 15 to 30 (King 1971).

5.3 *History of star formation and metal enrichment*

In order to completely specify the stellar content of a galaxy it is necessary to know the distribution of stellar ages and metal abundances, or equivalently the complete past history of star formation and metal enrichment at each radius. Fig. 5 shows the star formation rate as a function of time at five representative radii in Model D; the results for Models A–C are almost identical to Model D except that the curves are shifted to somewhat earlier times. The zero point of time for Fig. 5 is taken to be the beginning of the universal expansion, and the collapse of the protogalaxy is assumed to begin one free fall time later; this is the minimum time that would be required for a protogalaxy to expand from infinite density to a state of rest from which it can begin to collapse again.

Since the initial velocity dispersion is relatively small and the collapse is initially nearly a free fall, the protogalaxy develops a strong central density peak just one free fall time after the beginning of the collapse, i.e. at $t = 1{\cdot}2 \times 10^9$ yr. The star formation rate in the central region therefore rises rapidly to a maximum at this time. The star formation rate then begins to decrease as the protogalactic gas becomes depleted, but the decrease is less rapid in the nucleus than in the

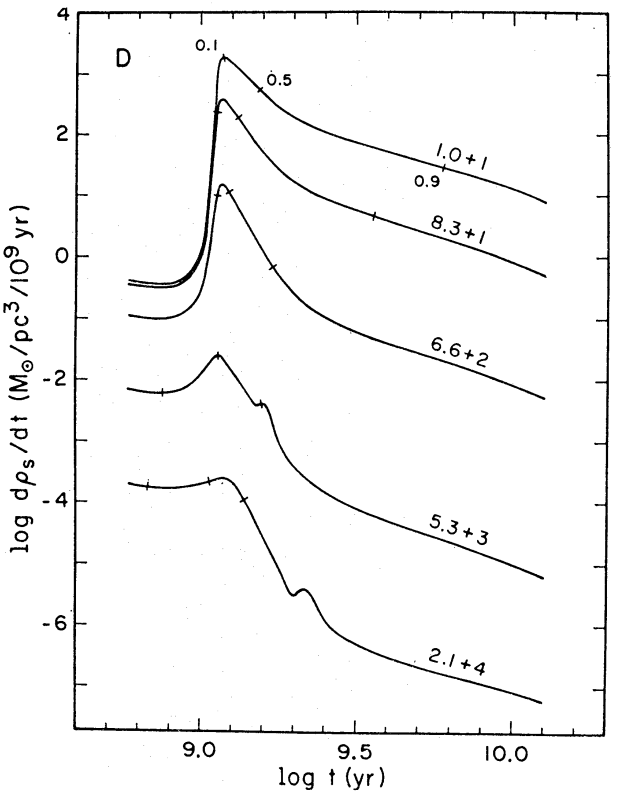

FIG. 5. *The star formation rate* vs. *time at five representative radii in Model D; the radius is indicated in pc on each curve. The quantity plotted is the formation rate in* $M_\odot$ *per* 10^9 *yr for those stars which at* $t = 12 \times 10^9$ *yr are located in a volume of* 1 pc^3 *at the indicated distance from the centre. The three ticks along each curve indicate the times at which star formation is* 10, 50 *and* 90 *per cent complete at each radius.*

outer regions because the residual gas, supplemented by recycled material, continues to condense toward the centre and form new stars there. The times at which star formation is 10, 50 and 90 per cent complete at each radius are marked along the curves in Fig. 5; we see that the halo of the galaxy (which contains the bulk of the mass) tends to form first, whereas the nucleus develops later and its formation continues for a considerably longer period of time. For the whole galaxy, star formation is 50 per cent complete at $t = 1{\cdot}1 \times 10^9$ yr and 90 per cent complete at $t = 1{\cdot}4 \times 10^9$ yr, whereas at a representative point in the nucleus with $r = 83$ pc the corresponding times are $1{\cdot}3 \times 10^9$ yr and $3{\cdot}7 \times 10^9$ yr. Over most of the galaxy the number of young stars still present after 12×10^9 yr is too small to have an important effect on the photometric properties, but the proportion of young stars increases toward the centre and this may have a significant effect on the photometric properties of the nucleus.

The time variation of the initial stellar metal abundance Z_f at the same radii is illustrated in Fig. 6. During the initial free fall collapse the metal abundance increases at about the same rate in all zones, but after a stationary background of stars has begun to form, the continuing inflow of gas produces a strong metal abundance gradient, as described in Section 5.2. In the nuclear region an approximate steady state situation is soon established in which the effects of metal production and continuing gas inflow nearly balance to produce a metal abundance distribution which remains nearly constant with time. The result that $Z(r)$ becomes nearly independent of time is similar to the prediction of the elementary argument of Larson (1972b), except that the latter neglected the existence of abundance gradients. In the outer part of the galaxy no such steady state is established since continuing star formation and metal production are not imporant there; during the later stages of evolution most of the gas in this region has been ejected from old,

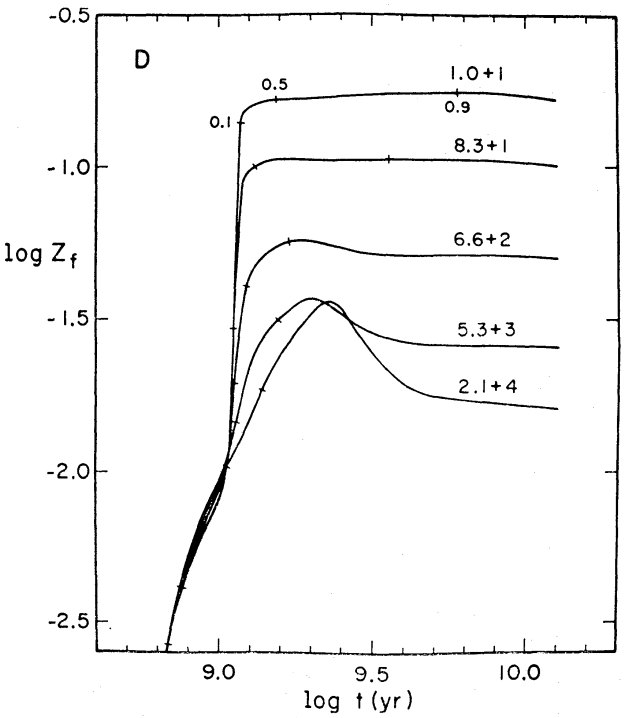

FIG. 6. *The initial stellar metal abundance Z_f vs. time at five radii in Model D. The curves are marked in the same way as those in Fig. 5.*

low mass stars, and therefore its metal abundance stops increasing after the initial rapid rise and drops again to a value more representative of the average Z with which the halo stars were formed. This effect has been noted previously in the (non-dynamical) galactic evolution models of Talbot & Arnett (1971), Ikeuchi *et al.* (1972), and others.

The distribution of stellar Z values in several zones at $t = 12 \times 10^9$ yr is illustrated in Fig. 7. The diagram shows $Z/Z_{\max}$, where $Z_{\max}$ is the maximum Z attained in each zone, plotted *vs.* N/N_1, the fractional number of stars formed up to any time t. An important result is that in zones near the centre ($r \lesssim 300$ pc) most

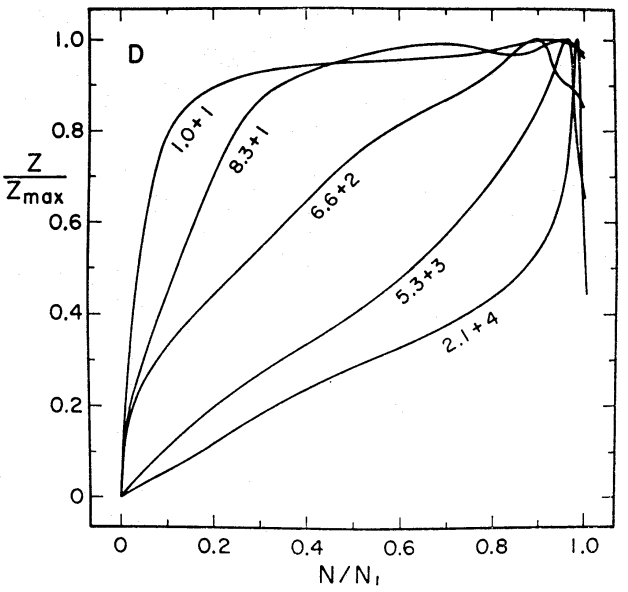

FIG. 7. *The distribution of stellar metal abundances at each of the five representative radii in Model D. Z is the metal abundance of stars formed at any time t at each radius and Z_{max} is the largest value ever attained by Z at that radius; N is the number of stars formed up to time t at each radius, and N_1 is the number formed up to time $t = 12 \times 10^9$ yr.*

of the stars in each zone have nearly the same metal abundance, and relatively metal poor stars are quite rate. Thus the proportion of stars with metal abundances smaller than $0{\cdot}1\ Z_{\max}$ is less than 10^{-2} at $r \lesssim 1$ kpc and less than 10^{-3} at $r \lesssim 20$ pc. This is an illustration of the ' chemically inhomogeneous collapse ' discussed by Searle (1973), who showed that if metal production occurs in a region of limited extent into which uncontaminated gas continues to flow, an approach to a uniform distribution of stellar Z values can be attained. It is well known that in the solar neighbourhood most of the stars have about the same Z, and metal poor stars are very rare; for example, Bond (1970) finds that stars with $Z \lesssim 0{\cdot}1\ Z_\odot$ occur with a frequency of only about one in 10^3. A qualitatively similar result has been found by van den Bergh (1971) for a region in the nucleus of our Galaxy. These observations, which cannot easily be understood on the basis of a simple ' one zone ' model of galactic evolution (Ostriker 1973), can be understood if the disc and nucleus of our Galaxy formed in the same manner as the nucleus of a spherical galaxy, i.e. through continuing inflow of gas into a region in which a nearly time-independent metal abundance distribution has been established. This general qualitative picture seems likely as a generalization of the present results for spherical models, and is

supported by some preliminary calculations for rotating models to be published later.

6. RESULTS WITH OTHER ASSUMPTIONS

6.1 *Effect of the assumed star formation rate*

Since the star formation rate is a crucial but uncertain function in the present models, it is of interest to consider the possibility of large deviations from the assumptions used in Models A–D for the star formation rate. In experimenting with other possible assumptions it has been found that the gaseous dissipation rate must be treated in a similar manner to the star formation rate, or else one process or the other may become strongly dominant and cause the resulting galaxy to be much too diffuse or much too condensed. Only two simple approaches were found to yield satisfactory models, namely the one used above in Models A–D and the one previously adopted in Paper I. To illustrate some of the possibilities, we present results for two additional models, Models E and F, which adopt the same initial stellar mass spectrum and the same boundary radius (50 kpc) as Model D but different assumptions for the star formation and gaseous dissipation rates.

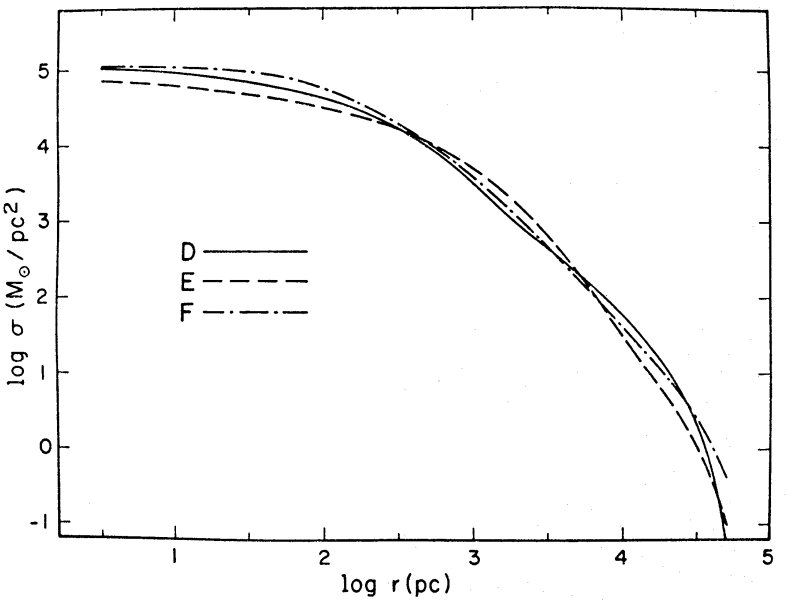

FIG. 8. *The projected density distributions of Models D, E and F.*

Since the star formation rate assumed in Models A–D is considerably higher than that inferred observationally for the solar neighbourhood or for spiral galaxies, the star formation and gaseous dissipation rates have been arbitrarily reduced by about a factor of 4 in Model E, which has $C_D = C_S = 0{\cdot}2$ and an initial velocity dispersion of 12 km s^{-1}. The projected density distribution $\sigma(r)$ and the projected metal abundance $Z_p(r)$ at time $t = 12 \times 10^9$ yr are shown in Figs 8 and 9, along with the results for Models D and F. The projected density $\sigma(r)$ decreases more rapidly with r (approximately as $r^{-2{\cdot}8}$) than is observed, so that Model E does not provide a very good model for NGC 3379 or most elliptical galaxies. A noteworthy feature of Model E is that the projected metal abundance $Z_p(r)$ does not become constant at large radii as in Model D but continues to decrease with increasing

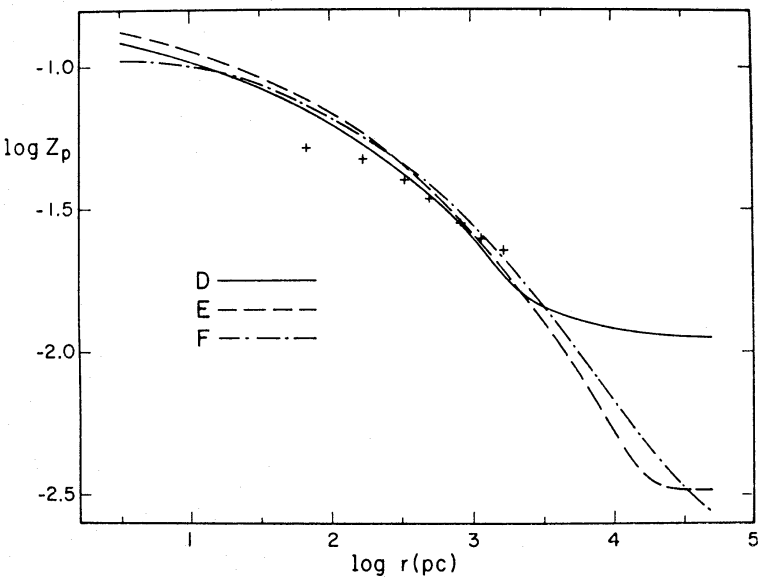

FIG. 9. *The projected average stellar metal abundance in Models D, E and F. The + symbols are reproduced from Fig. 4.*

radius (see Fig. 9). This is mainly because the relatively low star formation rate in Model E results in less star formation and therefore less metal production during the early stages of the collapse when the outermost part of the galaxy is formed.

A better fit to the observed surface brightness distribution of NGC 3379 (although still not quite as good as Model B) is provided by Model F, which is based on the same type of assumptions for the star formation and gaseous dissipation rates as were previously used in Paper I. The star formation rate is assumed to vary as a power of the gas density:

$$\frac{d\rho_s}{dt} = 0{\cdot}85\ \rho_g^{1{\cdot}85}, \tag{13}$$

and the gaseous dissipation rate is assumed to be given by equation (I.6) of Paper I. In order to obtain reasonable agreement with the surface brightness distribution of NGC 3379 it is necessary to assume a much larger initial velocity dispersion than in Models A–D, and a value of 55 km s^{-1} has been adopted here. The projected density and metal abundance distributions of Model F are illustrated in Figs 8 and 9. The metal abundance in Model F continues to decrease with increasing radius as in Model E and for a similar reason, since the star formation rate given by equation (13) is initially much smaller than that used in Model D. In addition, the large initial velocity dispersion in Model F inhibits any substantial inward motion of the stars once they have formed, so that a differential motion between gas and stars is present almost from the outset and this establishes a continuous Z gradient throughout the galaxy. Clearly, direct observations of the metal abundance in galactic halos would be valuable in helping to discriminate between models.

Fig. 10 shows the predicted line-of-sight velocity dispersions of Models D, E and F, averaged along lines of sight through the models. The velocity dispersions in the nuclei of Models D and F agree well with the velocity dispersion of 187 km s^{-1} observed in the nucleus of NGC 3379 (Burbidge *et al.* 1961). However, in the outer regions where the line-of-sight velocity dispersion reflects mainly the transverse velocity component, Models D and F diverge because of the larger initial

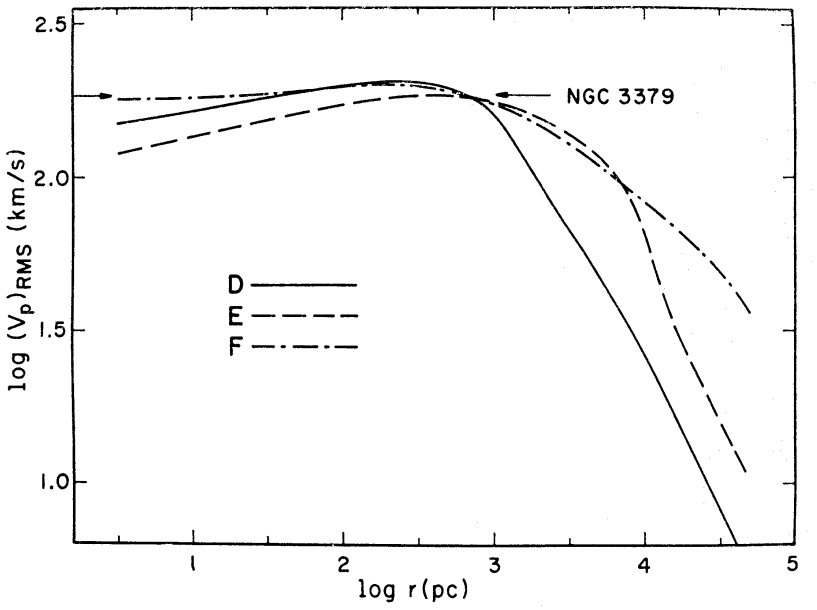

FIG. 10. *The line-of-sight velocity dispersion averaged along lines of sight through Models D, E and F, plotted* vs. *projected distance from the centre. The arrows indicate the velocity dispersion measured by Burbidge et al.* (1961) *in the nucleus of NGC* 3379 ($r \lesssim 200$ *pc*).

velocity dispersion in Model F, which produces a larger transverse velocity dispersion. In Model F the stellar velocity distribution is nearly isotropic throughout the system, in contrast to Model D where the velocity distribution is radially elongated. Again, measurements of the velocity dispersions in the outer parts of elliptical galaxies would be useful in helping to discriminate between models.

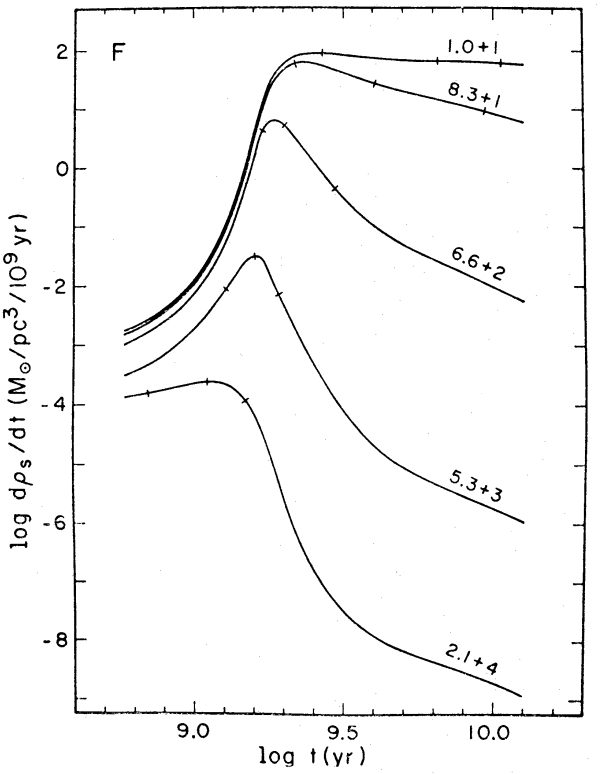

FIG. 11. *The star formation rate* vs. *time at five radii in Model F. The data presented are the same as those shown for Model D in Fig.* 5.

The star formation rates and initial stellar metal abundances at several radii in Model F are shown as a function of time in Figs 11 and 12, which may be compared with the results for Model D shown in Figs 5 and 6. The initial collapse is somewhat slower in Model F than in Model D because of the larger initial velocity dispersion, and the condensation of residual gas toward the centre and the formation of the nucleus take a longer time because the gaseous dissipation rate becomes relatively low at low gas densities. The star formation rate also becomes very low at low gas density, and therefore most of the residual gas condenses into the nucleus before becoming dense enough to form stars; thus the residual star formation activity in Model F is more strongly concentrated toward the centre than in Models A–E.

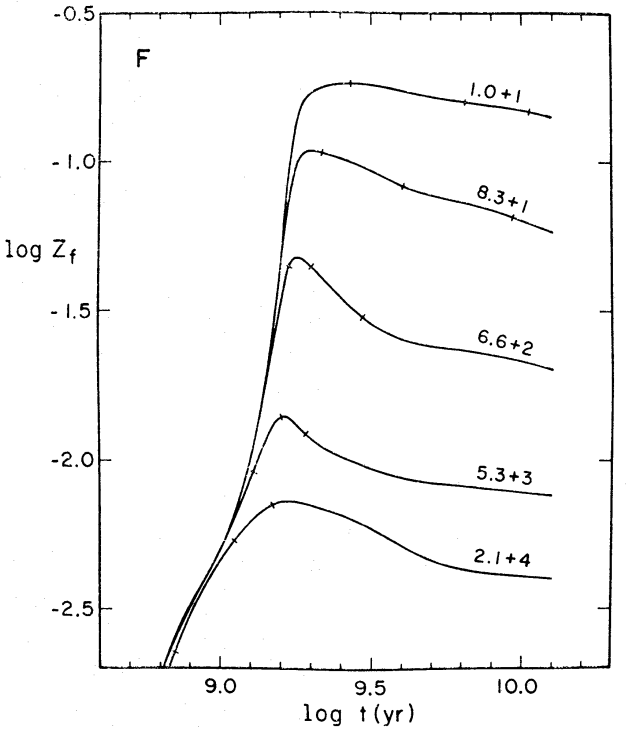

FIG. 12. *The initial stellar metal abundance Z_f* vs. *time at five radii in Model F.*

The final distribution of stellar Z values at several radii in Model F is illustrated in Fig. 13, which may be compared with the results for Model D shown in Fig. 7. While the results for Models D and F are quantitatively different, they share the basic qualitative property that in the inner part of the galaxy most of the stars at any point have approximately the same Z and metal poor stars are quite rare, whereas in the outer part of the galaxy the stars have a wider range of Z values.

Model F, with a total residual gas content after 12×10^9 yr of about $1{\cdot}4 \times 10^8\, M_\odot$, predicts more gas and more young stars in the nuclear region than are observed in most elliptical galaxies; however, this is not necessarily an objection to the basic model since there may in reality be processes which tend to remove the residual gas from elliptical galaxies (e.g. Mathews & Baker 1971). Also, some elliptical galaxies do contain significant amounts of gas and young stars; for example, NGC 4278 contains $\approx 6 \times 10^4\, M_\odot$ of gas within about 100 pc of the centre (Osterbrock 1971), which may be compared with the model predictions of

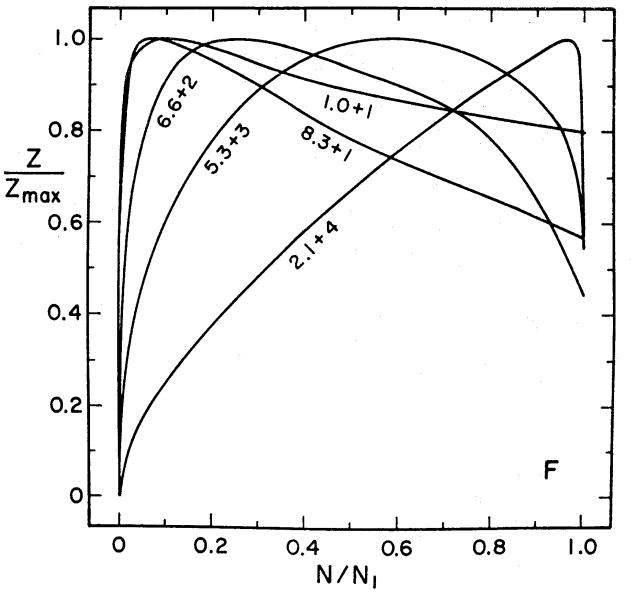

FIG. 13. *The distribution of stellar metal abundances at five radii in Model F.*

$2 \times 10^3\ M_\odot$ for Model D and $3 \times 10^5\ M_\odot$ for Model F in a region of the same size. Evidence for ongoing or recent star formation in the inner regions of a number of elliptical galaxies, as predicted by the present models (particularly Model F), has been described by van den Bergh (1972).

6.2 *Effect of an expanding boundary*

Since the assumption of a fixed boundary is rather arbitrary and not necessarily realistic in all cases, we have computed some models with an expanding boundary for which $R = R_0 t^{2/3}$. These models may crudely simulate not only the case of galaxy formation in an expanding region but also cases in which, for one reason or another, condensation of primordial material into a galaxy continues for a longer period of time than in the models so far considered. These 'expanding models' all have the same initial mass spectrum as Models B and D–F, i.e. a Salpeter law between 0·02 and 50 $M_\odot$, and the calculations have been started at $t = 10^8$ yr in each case.

Model G has been calculated using assumptions which are identical to Model E except that the boundary radius is $R = 1000\ t^{2/3}$ (R in pc, t in 10^6 yr). In this model expansion continues throughout the system until $t \simeq 5 \times 10^8$ yr, at which time $R \simeq 65$ kpc and the velocity dispersion has dropped to about 6 km s^{-1}; the conditions at this time are thus similar to the initial conditions for Model D, except that about 20 per cent of the mass has already been converted into stars. The central part of the protogalaxy then stops expanding and begins to collapse, and at successively later times shells farther and farther from the centre stop expanding and begin to fall inward. The central gas density and star formation rate rise rapidly to a maximum at $t \simeq 1{\cdot}2 \times 10^9$ yr, as in Model D, but the maximum is less pronounced than in Model D and the formation process continues for a longer time because of the ever increasing time required for the outermost layers of the protocloud to stop expanding and fall back into the galaxy. The final results are similar to those for Model D except that, as illustrated in Figs 14 and 15, the

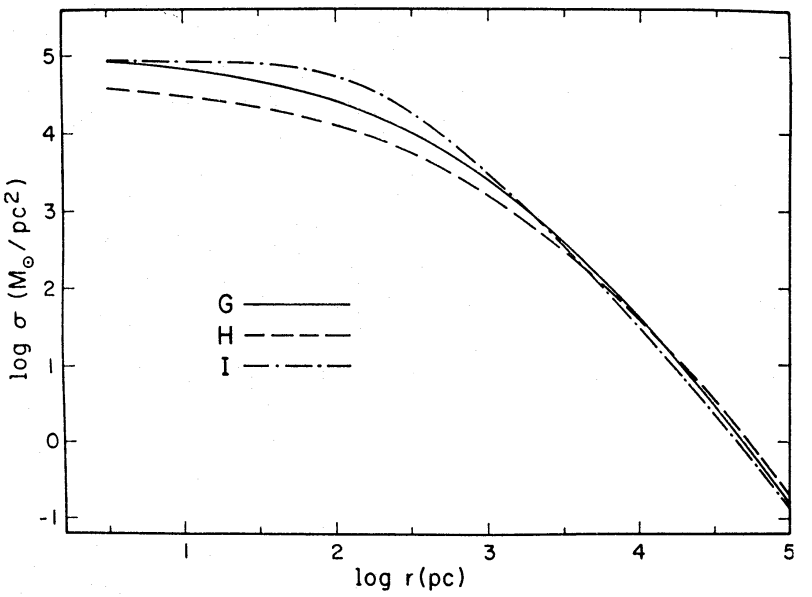

FIG. 14. *The projected density distributions of Models G, H and I.*

projected density $\sigma(r)$ and metal abundance $Z_p(r)$ fall off somewhat less rapidly at large radii. Note that while Model E (Section 6.1) had a density distribution which was too steep, the effect of an expanding boundary is to make the density distribution less steep and more realistic; for Model G we find approximately $\sigma(r) \propto r^{-2.0}$.

Model H, which is identical to Model G except that $R = 1100\, t^{2/3}$, represents a more extreme case of prolonged expansion and recollapse. The central region does not begin to collapse until $t \simeq 1.2 \times 10^9$ yr, and the peak gas density and star formation rate occur at $t \simeq 2.7 \times 10^9$ yr. The star formation rate drops relatively gradually after reaching its maximum (see Fig. 16), and even after 12×10^9 yr the galaxy still has an appreciable gas content (~ 12 per cent) and star formation

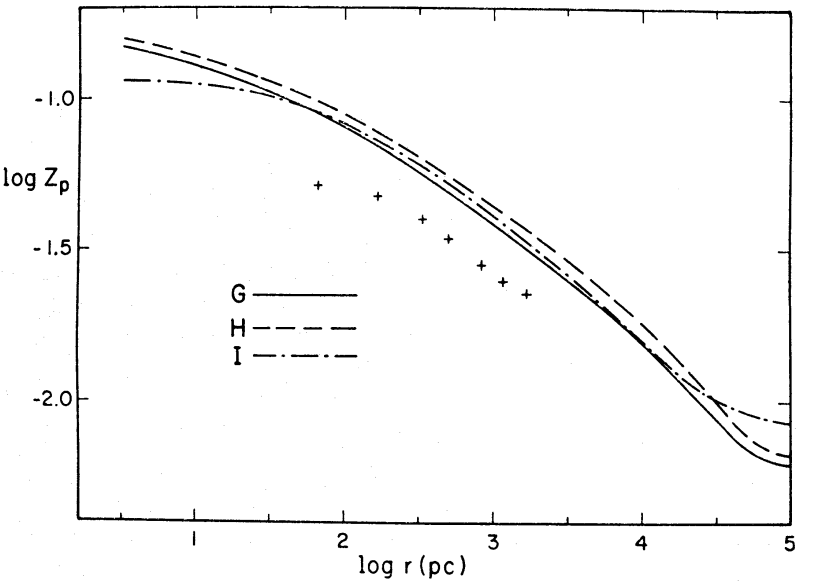

FIG. 15. *The projected average stellar metal abundance in Models G, H and I. The + signs are taken from Fig. 4.*

rate ($\sim 1{\cdot}6\, M_\odot\ \mathrm{yr}^{-1}$) due to the continuing infall of gas from the outer layers of the remnant protocloud. Thus Model H would clearly not look like a normal elliptical galaxy but would instead probably resemble an irregular or late spiral galaxy, at least as far as its gas and stellar content are concerned.

Finally, Model I has been computed with the same assumptions as Model F except that the boundary radius is $R = 1000\, t^{2/3}$. In this case the recollapse begins at $t \simeq 7 \times 10^8$ yr, and the total star formation rate reaches a broad maximum at $t \simeq 2 \times 10^9$ yr. The time dependence of the star formation rate at several radii in Model I is illustrated in Fig. 17, which may be compared with the results shown for Model H in Fig. 16. The tendency of residual gas to concentrate in the nucleus before forming stars is even more evident here than in Model F (Fig. 11); in fact, the

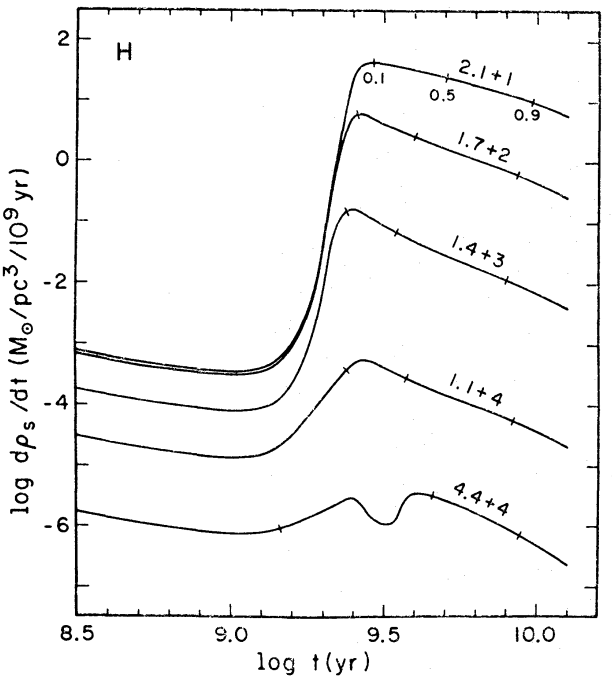

FIG. 16. *The star formation rate* vs. *time at five radii in Model H.*

gas density and star formation rate at the centre ($r \lesssim 20$ pc) continue to increase monotonically up to $t = 12 \times 10^9$ yr. Star formation is correspondingly less important in the outer part of the galaxy, which would thus look more like a normal elliptical galaxy. Thus the striking feature of Model I is that it would resemble an elliptical galaxy with very active star formation still going on in its nucleus. This situation bears a suggestive resemblance to the galaxies with active nuclei, and may be relevant to the interpretation of these objects (Section 7.2).

From the various results described in this paper it appears that the structure finally attained by a spherical galaxy is not strongly dependent on the initial or boundary conditions for the protogalaxy but instead is determined mainly by basic physical processes, especially the star formation and gaseous dissipation processes. On the other hand, the time dependence of star formation as well as the proportion of gas and young stars remaining after 12×10^9 yr can vary widely from case to case, depending on the initial and boundary conditions. In particular, the models

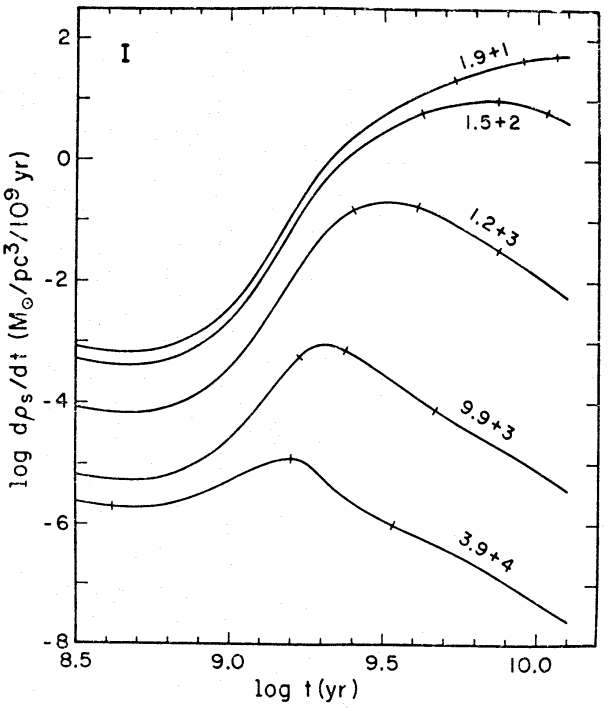

FIG. 17. *The star formation rate* vs. *time at five radii in Model I.*

described in this section show that under some circumstances the continuing condensation of protogalactic gas into a galaxy can support star formation at a rate of the order of 1 $M_\odot$ yr^{-1} or more for 12×10^9 yr or longer, a possibility which may help to explain some important characteristics of normal and peculiar galaxies (Larson 1972a).

7. POSSIBLE OBSERVATIONAL CONSEQUENCES OF GALAXY FORMATION

7.1 *The time of galaxy formation*

In any consideration of the observable consequences of galaxy formation a key role is played by the time (i.e. redshift) at which galaxy formation occurs. In the present models, the most conspicuous observable property of a forming galaxy would be the high luminosity produced by the many massive young stars formed; other conspicuous phenomena, such as the formation of luminous H II regions and the production of supernovae at a high rate, would also accompany the formation of massive stars. Since these stars have lifetimes of $\lesssim 10^8$ yr which are short compared with the time scale for formation of a galaxy ($\approx 10^9$ yr), the number of massive stars present at any time and hence the luminosity of a protogalaxy are approximately proportional to the star formation rate. For example, with a Salpeter mass spectrum between 0·02 and 50 $M_\odot$ as assumed in most of the present models, it can be shown that the luminosity due to main sequence stars is about 3×10^9 $L_\odot$ times the star formation rate in solar masses per year.

The time dependence of the total star formation rate in all of the present models is shown in Figs 18 and 19. The sudden 'turning on' of star formation when the calculations begin is of course an artificial feature of the models, but in all cases the star formation rate increases to a maximum about one free fall time

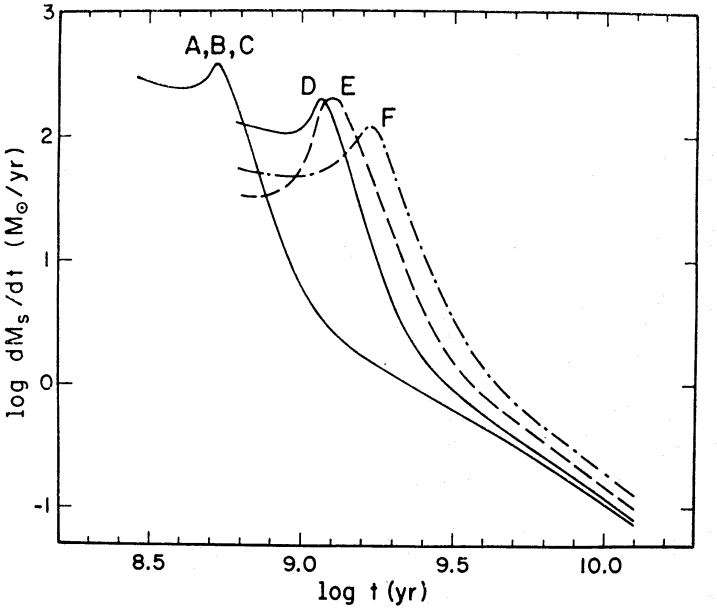

FIG. 18. *The total star formation rate* vs. *time for Models A–F.*

later when a strong central condensation develops. The time of maximum star formation rate and maximum luminosity varies from 5×10^8 yr for Models A–C to $2{\cdot}7 \times 10^9$ yr for Model H, a 'typical' value being about $1{\cdot}5 \times 10^9$ yr. The redshifts corresponding to these times depend sensitively on uncertain cosmological parameters, but if we adopt $H = 50$ km s^{-1} Mpc^{-1} and $q = \frac{1}{2}$, the corresponding range of redshifts is from 7·0 to 1·9, with a 'typical' value of about 3·3. The largest of these values should probably be regarded as an upper limit since it refers to models with a boundary radius of only 30 kpc, which is probably a lower limit for typical galaxies; at least some elliptical galaxies are observed to extend out to a radii of 50 kpc or more, and they must have collapsed at later times and smaller

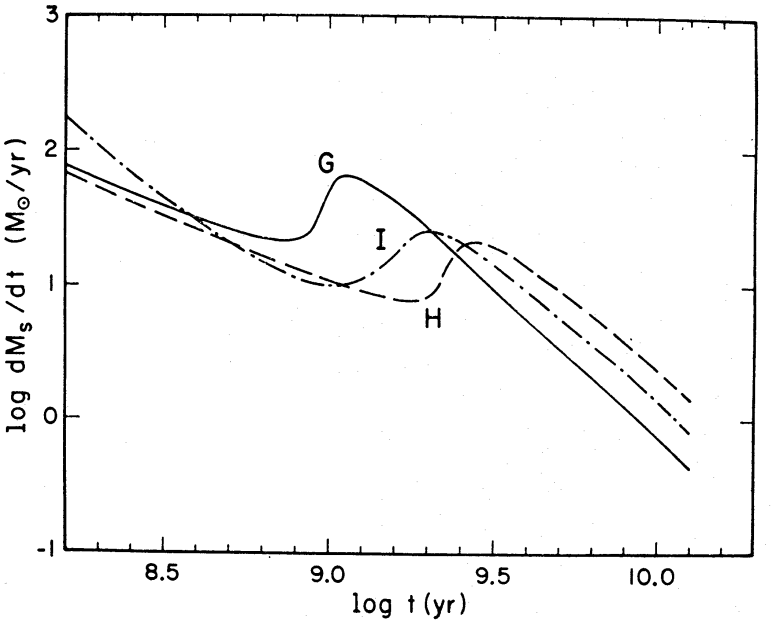

FIG. 19. *The total star formation rate* vs. *time for the 'expanding' Models G, H and I.*

redshifts than the models with $R = 30$ kpc. Thus redshifts in the lower part of the above range, say of the order of 2 to 5, may be most realistic. Smaller values are entirely possible, and there is no *a priori* reason why some protogalaxies should not collapse at even later times than any of the present models; thus galaxy formation may continue, presumably at a decreasing rate, down to the present time (i.e. to zero redshift).

We have so far discussed only the time of maximum star formation rate, but it is important to note that the galaxy formation process continues for a finite period of time which may be quite extended in some cases; thus the effects of galaxy formation may be observable over a considerable range of redshifts even in a single galaxy. This is particularly true of the 'expanding models' G–I, in which star formation continues at a significant rate even after 12×10^9 yr. It is also noteworthy that in all of the present models star formation continues for a relatively extended period of time in the nucleus, owing to the continuing inflow of residual gas into the nuclear region. Thus one might expect to see star formation continuing actively in the nuclear regions of some galaxies at redshifts which may be considerably smaller than the redshift at which the bulk of the galaxy formation activity took place.

7.2 *Possible interpretation of galaxies with active nuclei*

There is now good evidence (e.g. Gunn 1971; Kristian 1973; Sandage 1973) that quasars represent a particularly intense form of nuclear activity in large elliptical galaxies and that the quasars are thus morphologically as well as spectroscopically similar to the *N* galaxies and Seyfert galaxies, the basic phenomenon in all cases being the generation of large amounts of non-thermal radiation in a small region in the nucleus of a galaxy. Many theories have been proposed to explain the origin of this radiation, but most of them require the presence in the nucleus of a substantial amount of gas and/or recently formed massive objects such as massive stars (which rapidly evolve to produce supernovae and pulsars), supermassive objects, or black holes. A high gas content and a high star formation rate are in fact expected to be present in the nucleus of a galaxy during the later stages of the galaxy formation process when the bulk of the galaxy has already formed and the remaining gas is condensing strongly at the centre to form a dense nucleus. Thus an attractive possible interpretation of the quasars and similar objects is that they may represent a stage in the formation of a galaxy, specifically the formation of a dense nucleus by the condensation of residual gas at the centre.

Some approximate numerical coincidences lend support to this possible interpretation of quasars. The redshift range of ≈ 2–5 suggested above for the time of maximum star formation rate in a forming galaxy is approximately consistent with the redshift range of ≈ 2–3 in which the highest space density of quasars is observed, and the agreement may be even better if the quasars represent a somewhat later stage of the galaxy formation process, as may well be the case. The peak star formation rate in a forming galaxy of mass $10^{11} M_\odot$ is of the order of $100 M_\odot$ yr^{-1} (Figs 18 and 19), which implies a stellar luminosity of the order of $3 \times 10^{11} L_\odot$; for a massive elliptical galaxy of mass $10^{13} M_\odot$ the peak stellar luminosity would be as high as $\approx 3 \times 10^{13} L_\odot$. While these numbers cannot be compared directly with the (mostly non-thermal) radiation from quasars, they at least show that quasar-like luminosities are to be expected for forming galaxies. Finally, it has been noted by Schmidt (1972) that the space density of quasars at a redshift of 2·5 is

comparable with the presently observed space density (in comoving coordinates) of giant elliptical galaxies, a fact which is consistent with the interpretation of the quasars as an early stage in the evolution of giant elliptical galaxies.

It is possible that the various apparently exotic properties of quasars, such as the non-thermal emission, rapid variability, and complex and variable small scale radio structure, can be accounted for by relatively conventional processes if supernovae and pulsars are produced at a high rate in a dense ambient gas in the nucleus of a galaxy (Blandford & Rees 1972; Arons *et al.* 1973). This situation is expected to occur during the formation of a galactic nucleus, since a high rate of star formation leads very rapidly to a high rate of production of supernovae and pulsars. If all stars more massive than $4\,M_\odot$ become pulsars (Gunn & Ostriker 1970) and if we consider as before a Salpeter mass spectrum between 0·02 and $50\,M_\odot$, then a star formation rate of $100\,M_\odot\,\mathrm{yr}^{-1}$ yields a pulsar formation rate of $1\,\mathrm{yr}^{-1}$. If each supernova/pulsar releases 10^{53} erg and if most of this energy is converted into non-thermal radiation, the corresponding average luminosity is then about $10^{12}\,L_\odot$, or about three times the thermal luminosity from stars; thus the luminosity of a forming galactic nucleus could well be predominantly non-thermal. In the quasar model of Blandford & Rees (1972) and Arons *et al.* (1973), the low frequency electromagnetic waves produced by an assembly of pulsars accelerate electrons from the ambient gas to relativistic energies, causing them to radiate non-thermally the pulsar energy; with this model, the properties of typical quasars can be accounted for with a pulsar formation rate of ≈ 1–$10\,\mathrm{yr}^{-1}$, a rate which is easily achieved during the formation of a massive elliptical galaxy. The theory of Arons *et al.* (1973) requires most of the quasar activity to take place in a small volume of dimension only ~ 10 pc, a requirement which is not quantitatively met by the present models. However, the present models describe only the averaged or smoothed-out properties of a forming galaxy, and in reality the star formation process is almost certainly highly non-uniform and confined mostly to small regions of exceptionally high density; it is probably in such atypically small, dense regions that the conditions required for quasar activity are met.

The fact that quasars and similar objects are observed over a wide range of redshifts extending down to nearly zero can plausibly be understood as being due to the continuing formation of galaxies at all times up to the present time. The strong variation in the space density of quasars as a function of redshift (Schmidt 1972) would then indicate a strong decrease in the galaxy formation rate with time, a situation which is not implausible. However, it is also possible that quasar activity may sometimes occur in a galaxy long after the initial collapse process if a remnant part of the initial protocloud or another cloud of intergalactic matter falls into the galaxy and condenses in the nucleus to produce a high rate of star formation there (Larson 1972a). If this is an important cause of quasar activity, then the quasar redshift distribution would reflect at least in part a decrease in the rate of occurrence of such delayed infall processes, which again is to be expected since the density of protogalactic matter or intergalactic clouds decreases with time. At present our knowledge about quasars is not sufficient to indicate just how closely the quasar phenomenon is related in time to the initial collapse of the protogalaxy. The large redshifts of most quasars indicate that in most cases the quasar phenomenon occurs at an early stage in the evolution of a galaxy, but in some nearby galaxies showing nuclear activity it appears that the galaxy involved is basically a normal old galaxy, so that in some cases there is evidence for continuing or recurrent

nuclear activity long after a galaxy has formed. Much more observational work will be required to completely elucidate the relation between nuclear activity and the formation and evolution of galaxies.

8. CONCLUSIONS

The present results, particularly for Models B and D, demonstrate that collapse models based on simple assumptions and plausible choices of parameters are able to reproduce rather well the principal observed properties of nearly spherical galaxies; the properties satisfactorily explained by the models include the surface brightness distribution, the metal abundance distribution, and the photometric properties of nearly spherical galaxies. Thus the conventional collapse picture of galaxy formation represented by these models is able to give a quite satisfactory account of the formation of such galaxies, and there is no need to invoke any of the more exotic or unconventional theories which have sometimes been proposed, such as the idea that galaxies may be formed by the ejection of matter from a nuclear source. Indeed, the metal abundance gradients observed in galactic nuclei are most naturally explained in terms of a collapse or infall process, and it is difficult to explain the distribution of stellar metal abundances in the solar vicinity in any other way (e.g. Ostriker 1973).

The models suggest that the star formation rate in a collapsing protogalaxy reaches a maximum at a time of the order of $1{\cdot}0$–$2{\cdot}5 \times 10^9$ yr after the big bang, corresponding to a redshift of the order of 2 to 5, and that the collapse process takes a similar amount of time for its completion. As the system evolves, the residual gas tends to become more and more condensed at the centre, so that intense star formation activity may continue in the nucleus of the galaxy for a significantly longer period of time. Within the uncertainties, the results are consistent with the interpretation of the quasar phenomenon as a stage in the formation of a giant elliptical galaxy, namely the stage when a dense nucleus is forming as a result of the central condensation of residual gas. The complete explanation of the quasar phenomenon evidently involves many complicated physical processes and it is not yet possible to make quantitative predictions for all of these processes, but the present interpretation (see also Arons *et al.* 1973) at least does not seem inconsistent with any present knowledge, and it is again not clear that any more exotic or unconventional models are required.

The present models do not provide any direct explanation for the apparent correlation between the masses and the metal abundances of elliptical galaxies, since the fractional mass processed into heavy elements is fixed within fairly narrow limits by the assumed stellar mass spectrum, regardless of the dynamical characteristics of the models. As long as a galaxy can be treated as a closed system, the effect of the internal dynamics is mainly to redistribute the heavy elements without significantly changing the total amount produced. Thus in order to explain differences in the metal abundances of galaxies it is necessary either to assume different initial mass spectra, for which there is no obvious justification, or to abandon the assumption of a closed system and allow that forming galaxies may lose or gain processed gas from their surroundings. For example, if galaxies of different masses form at the same time and in the same region of space, e.g. in a protocluster of galaxies, it is not difficult to imagine that the small galaxies will tend to lose their processed gas and that the massive galaxies will tend to accrete this metal-enriched

gas from the surrounding region. This might then account for the fact that more massive galaxies tend to have higher metal abundances. At any rate, it seems likely that future more sophisticated models of galaxy evolution will have to allow for the fact that galaxies need not evolve as closed systems but may exchange matter with their surroundings.

Yale University Observatory, New Haven, Connecticut 06520

REFERENCES

Arons, J., Gunn, J. E., Kulsrud, R. M. & Ostriker, J. P., 1973. In preparation.
Bergh, S. van den, 1971. *Astr. J.*, **76,** 1082.
Bergh, S. van den, 1972. *J. R. astr. Soc. Canada*, **66,** 237.
Blandford, R. D. & Rees, M. J., 1972. *Astrophys. Lett.*, **10,** 77.
Bond, H. E., 1970. *Astrophys. J. Suppl.*, **22,** 117.
Burbidge, E. M., Burbidge, G. R. & Fish, R. A., 1961. *Astrophys. J.*, **134,** 251.
Faber, S. M., 1973. *Astrophys. J.*, **179,** 731.
Field, G. B., 1964. *Astrophys. J.*, **140,** 1434.
Field, G. B., 1974. To be published in *Galaxies and the Universe* (*Stars and Stellar Systems*, Vol. IX), eds A. & M. Sandage. University of Chicago Press.
Gott, J. R., 1973. *Astrophys. J.*, in press.
Gunn, J. E., 1971. *Astrophys. J. Lett.*, **164,** L113.
Gunn, J. E. & Ostriker, J. P., 1970. *Astrophys. J.*, **160,** 979.
Ikeuchi, S., Sato, H., Sato, T. & Takeda, H., 1972. *Prog. theor. Phys.*, **48,** 1885.
Jones, B. J. T., 1973. *Astrophys. J.*, **181,** 269.
King, I. R., 1966. *Astr. J.*, **71,** 64.
King, I. R., 1971. *Publ. astr. Soc. Pacific*, **83,** 377.
Kristian, J., 1973. *Astrophys. J. Lett.*, **179,** L61.
Larson, R. B., 1969. *Mon. Not. R. astr. Soc.*, **145,** 405 (Paper I).
Larson, R. B., 1972a. *Nature*, **236,** 21.
Larson, R. B., 1972b. *Nature, Phys. Sci.*, **236,** 7.
Larson, R. B., 1973. *Mon. Not. R. astr. Soc.*, **161,** 133.
Larson, R. B. & Starrfield, S., 1971. *Astr. Astrophys.*, **13,** 190.
Mathews, W. G. & Baker, J. C., 1971. *Astrophys. J.*, **170,** 241.
McClure, R. D., 1969. *Astr. J.*, **74,** 50.
Miller, R. H. & Prendergast, K. H., 1962. *Astrophys. J.*, **136,** 713.
Osterbrock, D. E., 1971. In *Nuclei of galaxies*, p. 151, ed. D. J. K. O'Connell, American Elsevier, New York.
Ostriker, J. P., 1973. In preparation.
Rees, M. J., 1971. *General relativity and cosmology*, p. 315, ed. R. K. Sachs, Academic Press, New York.
Sandage, A. R., 1972. *Astrophys. J.*, **176,** 21.
Sandage, A. R., 1973. *Astrophys. J.*, **180,** 687.
Saslaw, W. C., 1972. *Astrophys. J.*, **177,** 17.
Schmidt, M., 1972. *Astrophys. J.*, **176,** 303.
Searle, L., 1973. In *l'Âge des Étoiles* (*IAU Colloquium No.* 17), ed. G. Cayrel de Strobel & A. M. Delplace, Observatoire de Paris — Meudon.
Shu, F. H., Milione, V., Gebel, W., Yuan, C., Goldsmith, D. W. & Roberts, W. W., 1972. *Astrophys. J.*, **173,** 557.
Silk, J. & Ames, S., 1972. *Astrophys. J.*, **178,** 77.
Spinrad, H., Gunn, J. E., Taylor, B. J., McClure, R. D. & Young, J. W., 1971. *Astrophys. J.*, **164,** 11.
Spinrad, H., Smith, H. E. & Taylor, D. J., 1972. *Astrophys. J.*, **175,** 649.
Talbot, R. J. & Arnett, W. D., 1971. *Astrophys. J.*, **170,** 409.
Talbot, R. J. & Arnett, W. D., 1973. *Astrophys. J.*, **186,** 51.
Tinsley, B. M., 1972a. *Astr. Astrophys.*, **20,** 383.
Tinsley, B. M., 1972b. *Astrophys. J.*, **178,** 319.
Walker, M. F., 1962. *Astrophys. J.*, **136,** 695.
Weistrop, D., 1972. *Astr. J.*, **77,** 849.